ACS APPLIED MATERIALS & INTERFACES

Highly Sensitive Hydrogen Sensor Based on an Optical Driven Nanofilm Resonator

Junxian Luo, Shen Liu,* Peijing Chen, Yanping Chen, Junlan Zhong, and Yiping Wang

Cite This: *ACS Appl. Mater. Interfaces* 2022, 14, 29357−29365

Read Online

ACCESS | Metrics & More | Article Recommendations | Supporting Information

ABSTRACT: Nanofilm resonators combine ultracompact and highly mechanically sensitive properties, making them intriguing devices for sensing applications. For trace hydrogen detection, we demonstrate an optomechanical nanofilm resonator by employing a Pd- and Au-decorated graphene onto a fiber end facet. The Pd layer is a sensitive layer for selective absorption of hydrogen. Hydrogen sensing is achieved by all-optical measuring of the resonant frequencies shift of the optomechanical nanofilm resonator induced by hydrogen-related mechanical stress change. Using the approach, we realize highly sensitive hydrogen sensing at room temperature with a low detection limit, challenging the state-of-the-art. When the measured hydrogen concentration increases from 0 to 1000 ppm (v/v), the mechanical resonance frequencies of the sensor at 511.7 kHz, 1253.4 kHz, and 2231.7 kHz blue-shift by 100.4 kHz, 257.5 kHz, and 400.6 kHz, respectively. The response and recovery time are 120.3 and 91.3 s at a 1000 ppm hydrogen concentration. Such a sensor exhibits a low detection limit of 741 ppb and good repeatability in the measurement process, which makes the practical application of the sensor possible.

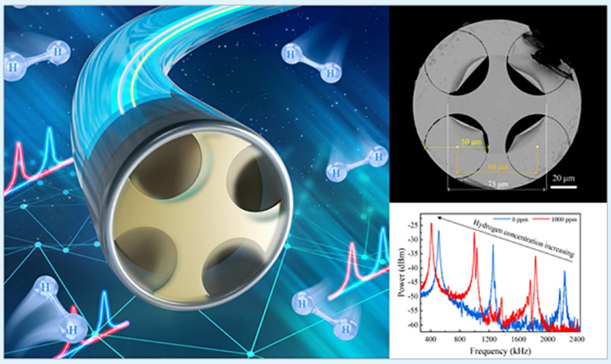

KEYWORDS: *optomechanical resonator, hydrogen sensor, optical fiber sensor, palladium, nanofilm*

1. INTRODUCTION

Micro- and nanoelectromechanical systems (MEMS and NEMS) actuate mechanical modes of micro- or nano-resonators electrically and exhibit great promise in the detection of mass,[1,2] spin,[3] and gas.[4] Due to the small spring constant and low effective mass of micro- and nanomechanical resonators, even very weak forces (e.g., including gas-induced effects) acting on them or small masses attached to their surface can considerably change their dynamics. Therefore, such devices can be used to measure forces with ultrahigh precision, finding numerous industrial applications including gas leakage detection. Compared with an electronic drive, optical actuation directly drives the mechanical vibration of film resonators using a modulated continuous laser or pulse laser instead of setting an extra conductive layer on the resonator surface in conjunction with an electric current to induce force. Dolleman et al. demonstrated an optical driven graphene squeeze-film mechanical resonator for gas pressure sensing by measuring the resonant frequency shifts induced by resonator stiffness change, and obtained a high responsivity of 9 kHz/mbar.[5] Additionally, the optical driven method can realize the selective actuation or suppression of the certain mechanical modes of nanofilm resonators. Some high-order mechanical modes exhibit high sensitivity to weak force. Waggoner et al. proposed a specially designed trampoline film resonator and demonstrated that some high-order modes perform better in low-level gas pressure measurement.[6] Considering the aforementioned advantages, optical actuation has been widely used in the studies of nanomaterial mechanical properties,[7] nonlinear vibration of resonators,[8] switching to tapping mode in atomic force microscopy imaging,[9] and development of highly sensitive bolometers.[10]

The sensitivity and specificity of nanofilm devices are crucial for gas sensing.[11,12] A previous study proposed an electrostatically driven composite film for the detection of volatile gases.[13] The result suggested that a significant impact of analyte sorption on the prestress of the composite film resulting in a resonance frequency shift. Thus, utilizing adsorption induced resonance frequency shift of films as the transduction mechanism has the potential to develop highly sensitive gas sensors. Besides, gas identification can be achieved by measuring the mechanical resonance of graphene nanofilm in all-optical manner. The pressure relaxation time of different gases can be directly measured by studying the vibration of a membrane with a nanopore perforation below the resonance

Received: March 6, 2022
Accepted: June 6, 2022
Published: June 15, 2022

https://doi.org/10.1021/acsami.2c04105

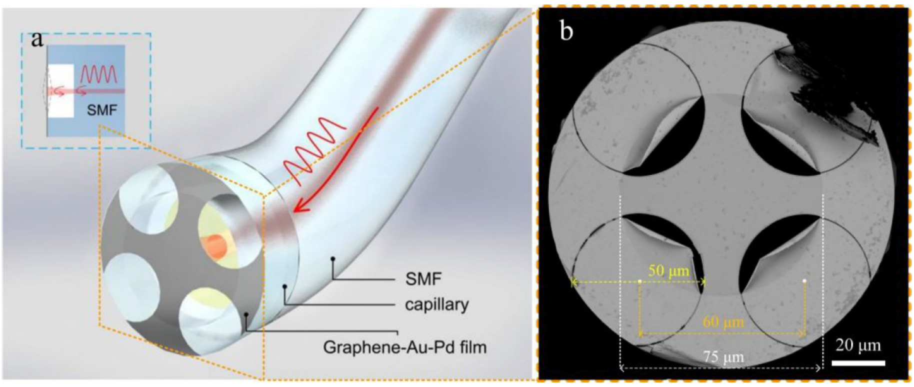

Figure 1. (a) Schematic of the proposed optomechanical hydrogen sensor. The inset shows a section schematic to illuminate the vibrational state of the nanofilm resonator. (b) SEM image of the graphene−Au-Pd nanofilm resonator covering the fiber end facet.

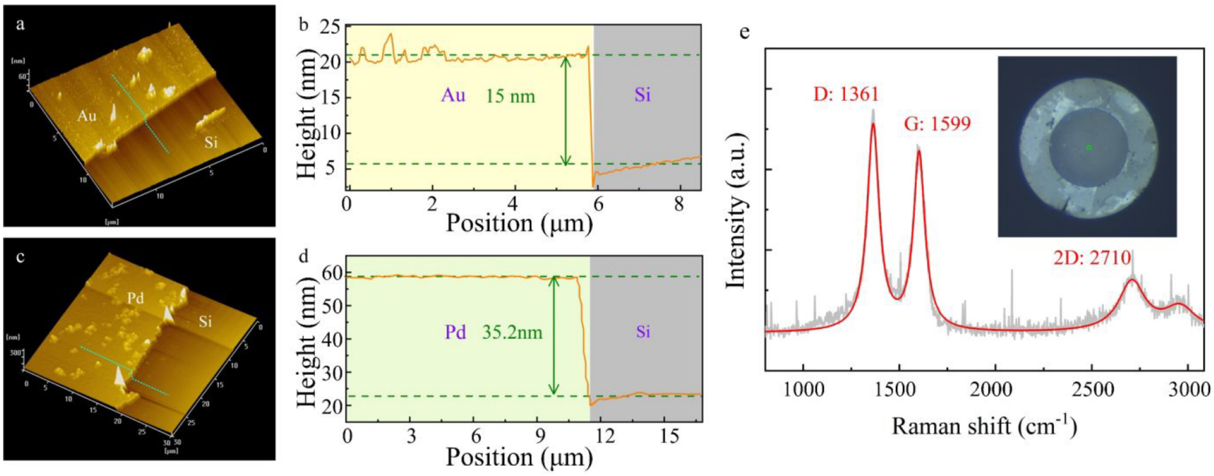

Figure 2. (a) The 3D Atomic force microscope (AFM) image of the Pd film on silicon (Si) wafer. (b) The height profile of Au film. (c) The 3D AFM image of the Pd film on Si wafer. (d) The height profile of Pd film. (e) Raman spectrum from suspended multilayer graphene measured using a 532 nm laser; The inset shows the microscopic image of multilayer graphene-covered fiber-tip end facet.

frequency. The pressure relaxation time can be affected by the permeation rate of the gases to be tested, which enables the recognition of specific gas.[14,15] Alternatively, the specificity of gas sensors can be realized based on the selection of sensitive materials. Materials such as rGO-ZnO-Pt composite film, CeO_2−SnO_2 nanoparticles, NiO-Nb_2O_5 nanoparticles, etc., are shown to have good selective absorption of hydrogen.[16−18] In addition, palladium (Pd) is one of the most commonly used modifiers in hydrogen sensing. The responses of Pd-decorated hydrogen sensors to common gases such as O_2, CO, CO_2, He, CH_4, NH_3, water vapor, acetone gas, and ethanol gas is far less than hydrogen.[19−22] Since hydrogen is flammable, detection with an electronic sensor carry the risk of local explosions caused by electric sparks. Comparetively speaking, all-optical sensor is a much safer and more competent solution for hydrogen measurements due to its chemical inertness and the absence of electrical arcing.[23−26]

An all-optical optomechanical hydrogen sensor on an integrated optical fiber platform is proposed and experimentally demonstrated in this paper. A section of a short capillary was spliced with a single mode fiber (SMF), whose end facet was sensitized by a trampoline-shaped graphene−Au-Pd layered nanofilm mechanical resonator to form a fiber-optic Fabry−Perot interferometer (FPI). The mechanical vibration of the resonator was driven by a sine-sweep modulated laser and probed by a continuous wave laser. In the hydrogen sensing experiments, the Pd film could reversibly transform lattice expansion into a metal hydride when exposed to hydrogen, which results in lower resonance frequencies. The hydrogen concentration could be resolved by measuring the shift in the resonance frequencies. The optomechanical hydrogen sensors exhibited good repeatability, possessed a high sensitivity, and showed a LOD of hundreds of parts per billion (ppb, v/v).

2. EXPERIMENTAL SECTION

2.1. Sensor Design and Fabrication. Previous work has identified that the pretensions in drumhead nanofilm mechanical resonators are usually very different, which leads to a lack of repeatability in the fabrication of nanofilm mechanical resonators.[27,28] Shape-tailoring drumhead nanofilms via FIB milling can improve fabrication repeatability in comparison to conventional drumhead resonators, in terms of the mechanical Q factor, resonance frequencies, and force sensitivities. Moreover, shape tailoring can partly release tension to obtain low-tension suspended structures, which were found to display increases in the mechanical Q factor along with a reduced damping coefficient.[29] Here, we used focused ion beam (FIB) milling technology to fabricate a trampoline-shaped suspended nanofilm, which was processed along a circular path rather than straight lines so that the nanofilm resonator was not easily damaged during processing and use. Figure 1a illustrates the schematic of the proposed optomechanical hydrogen sensor.

The fabrication process is as follows:

First, a section of capillary (75 μm internal diameter) was spliced to an SMF end facet, and then the hollow-core fiber (HCF) with a short length of 20−50 μm was cleaved. A short hollow cavity length can reduce optical divergence losses of sensors.

Second, the SMF end facet was coated with a layer of Au film via magnetron sputtering. In coating process, a silicon wafer was placed adjacent to the optical fiber at the same height with fiber end facet. Figure 2a shows the 3D atomic force microscope (AFM) image of the silicon wafers which were coated Au film. Figure 2b shows the height profiles along the green line in Figure 2a, which can be used to estimate the thickness is ∼15 nm. Au film can improve the reflectivity of an SMF end facet.

Third, multilayer graphene (6Carbon Technology, chemical vapor deposition method) was transferred to the HCF end facet and suspended. The transfer details see the "Methods" section. The Figure. 2e shows a Raman spectrum gathered from a transferred suspended graphene onto a capillary end facet. The experimental data was fitted using the Lorentz fitting method plot in red line. It is found that the wavenumbers of the three characteristic peaks of graphene are calculated to be 1361 cm^{-1}, 1599 cm^{-1}, and 2710 cm^{-1} respectively. The energy difference between the D and G peaks is corresponding to ∼seven layers of graphene.[30] The inset is the microscopic image of graphene-covered fiber-tip end facet, where the green circle shows the selected area for the Raman spectroscopy. The selected area was illuminated with a 532 nm laser for 15 min. Subsequently, the suspended graphene as a support layer, a layer of ∼15 nm thick Au film was coated onto it using the same parameters as the last step to improve the device reflectivity and improve the visibility of the film under scanning electron microscopy (SEM).

Fourth, the suspended film was patterned into a trampoline shape by irradiative milling with an FIB, as shown in Figure 1b. The trampoline shape was obtained by milling four circles with a diameter of 50 μm in the suspended film, and the distance between the centers of two adjacent circles was 60 μm, as shown in Figure 1b. The milling process was accomplished with a commercial gallium FIB operated under vacuum at 30 kV and with 10 pA ion currents to ensure that the film was completely penetrated and minimize damage due to the spread of the ion beam. Besides, coating the Au layer on the graphene film can make less breakage occur on the nanofilm during milling with the FIB.

Finally, a layer of Pd film was deposited onto the nanofilm for sensitivity to hydrogen. In the previous reports, the selective absorption of Pd have been demonstrated that Pd decorated sensors are much more responsive to hydrogen than many other common gases.[19−22] The Pd film can reversibly undergo lattice expansion to transform a metal hydride when exposed to hydrogen. Figure 2c shows the 3D AFM images of the silicon wafers which were coated Pd film with the same thickness. Figure 2d shows the height profiles along the green lines in Figure 2c. The total thickness of the Pd film is ∼35 nm.

As shown in the left inset of Figure 1a, the two reflectors (SMF end facet and suspended nanofilm) at the fiber tip form a fiber-optic FPI. Figure 3 shows the reflection optical spectrum of the FPI, in the range of 1500−1575 nm.

2.2. Experimental Setup. The experimental setup is depicted in Figure 4, where the spectrum of the FPI was measured from port 1 by a circulator, a broadband source (BBS), and an optical spectrum analyzer (OSA) with a resolution of 0.02 nm. After the optical spectrum of the FPI was measured, the nanofilm was a mechanical resonator whose mechanical vibration was actuated and measured through port 2: The drive laser λ_1 with a center wavelength of 1549.7 nm was modulated by an electro-optic modulator (EOM), which was driven by a sine-sweep signal from 300 kHz to 2400 kHz. The modulated λ_1 passed through a 9:1 coupler and circulator into the FPI to actuate the mechanical vibration of the nanofilm and was finally blocked by a bandpass filter. The probe laser λ_2 was set at 1549.7 nm, close to the point at half-maximum of the optical resonance. The probe laser λ_2 was passed through the coupler and the circulator and reflected by the film and then passed through the bandpass filter into a fast photoelectric detector (PD). The phase difference between the light beams reflected by the fiber end facet and the film, which changes due to the vibration of the optomechanical nanofilm resonator, induces the reflected light intensity λ_2 to be modulated by the vibration signal. The PD converts the light intensity signal into an electrical signal that is fed to a frequency spectrum analyzer (FSA) to measure the mechanical frequency properties of the optomechanical nanofilm resonator.

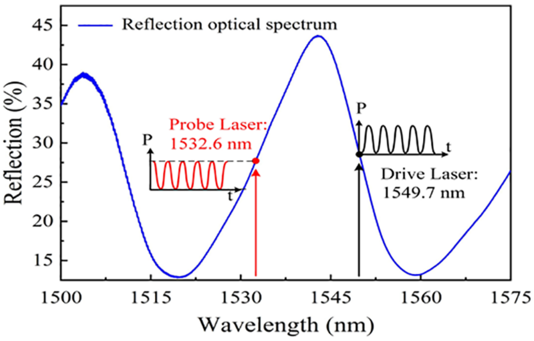

Figure 3. Reflection optical spectrum of the Fabry−Perot interferometer with a trampoline-shaped graphene−Au-Pd nanofilm.

The right part of Figure 4 shows the hydrogen concentration control setting. For the hydrogen concentration measurements, a certain hydrogen concentration was obtained by controlling the volume ratio of 0.2 vol % hydrogen (a mixture of nitrogen and hydrogen) to pure nitrogen using a computer and three mass flow controllers (MFCs, Seven Star, CS200) whose control error was less than ±1%. The pure nitrogen was controlled by the MFC with a full control range of 500 standard cubic centimeters per minute (SCCM). The 0.2 vol % hydrogen was controlled by the MFC with a full control range of 500 SCCM for the measurement of the 100 to 1000 ppm hydrogen concentrations. An MFC with the full control range of 10 SCCMs was used for the measurement of the 20 and 40 ppm hydrogen concentrations. N_2 and H_2 with a certain volume ratio were mixed in a gas chamber and flowed out through a plastic tube (3 mm internal diameter); the sensor was fixed in the plastic tube to detect changes in the hydrogen gas concentration. During this experiment, the total gas flow was set to 500 SCCM. By calculation, the gas concentration error of 20, 40, 100, 200, 400, 600, 800, and 1000 ppm are ±0.6 ppm, ± 0.8 ppm, ± 20 ppm, ± 20 ppm, ± 20 ppm, ± 20 ppm, ± 20 ppm, and ±20 ppm, respectively.

3. RESULTS AND DISCUSSION

3.1. Optomechanical Frequency Response. Figure 5 shows the mechanical frequency properties of the optomechanical nanofilm resonator using a 289.1 μW drive laser actuated in the FSA. We used finite element simulation software to simulate these three modes with the corresponding mode profiles shown in the inset. The mode-shapes are labeled as (m,n), where m refers to the number of nodal diameters and n to the number of nodal circles. The mechanical modes at 511.7 kHz (fundamental mode), 1.35 and 2.23 MHz are (0,1) mode, (1,1) mode, and (0,2) mode, respectively. There are two peaks observed in the (1,1) mode and (0,2) mode, which are the result of split degenerate modes usually caused by asymmetric or defective films.[31]

The mechanical frequency responses of the optomechanical nanofilm resonator were measured as the drive laser power increased from 129.7 to 319.2 μW. The test results are shown in Figure 6. The signal-to-noise ratio of the sensor frequency response characteristics increased with the drive laser power. At the same time, an actuated power-dependent decrease in the mechanical resonant frequency was observed, which, due to a negative detuning from the optical modification of the

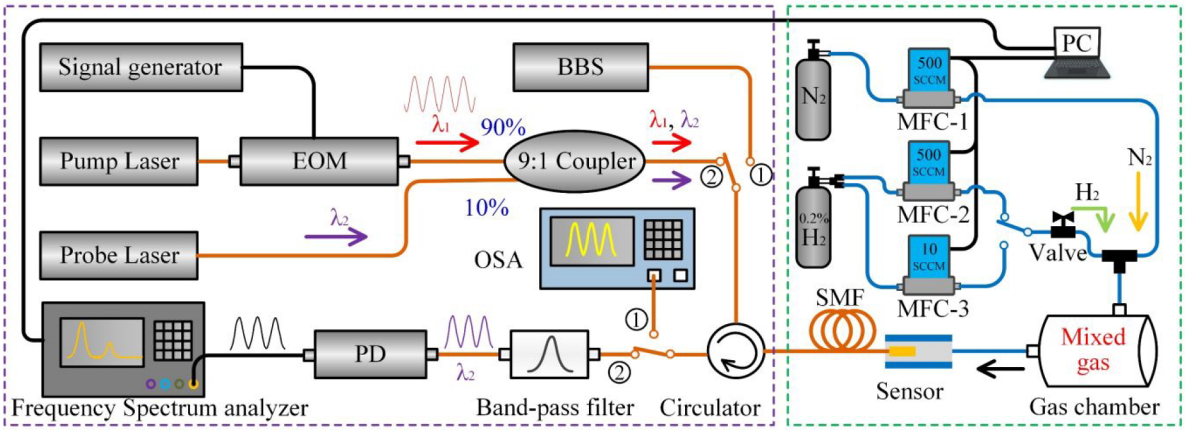

Figure 4. Layout of scientific instruments for characterizing the sensor's optical spectrum, mechanical frequency character and frequency response to different hydrogen concentrations. Port 1 and port 2 were used to measure the optical spectrum and mechanical frequency characteristics of the sensor, respectively. The right handside section of the setup is used to control the hydrogen concentration.

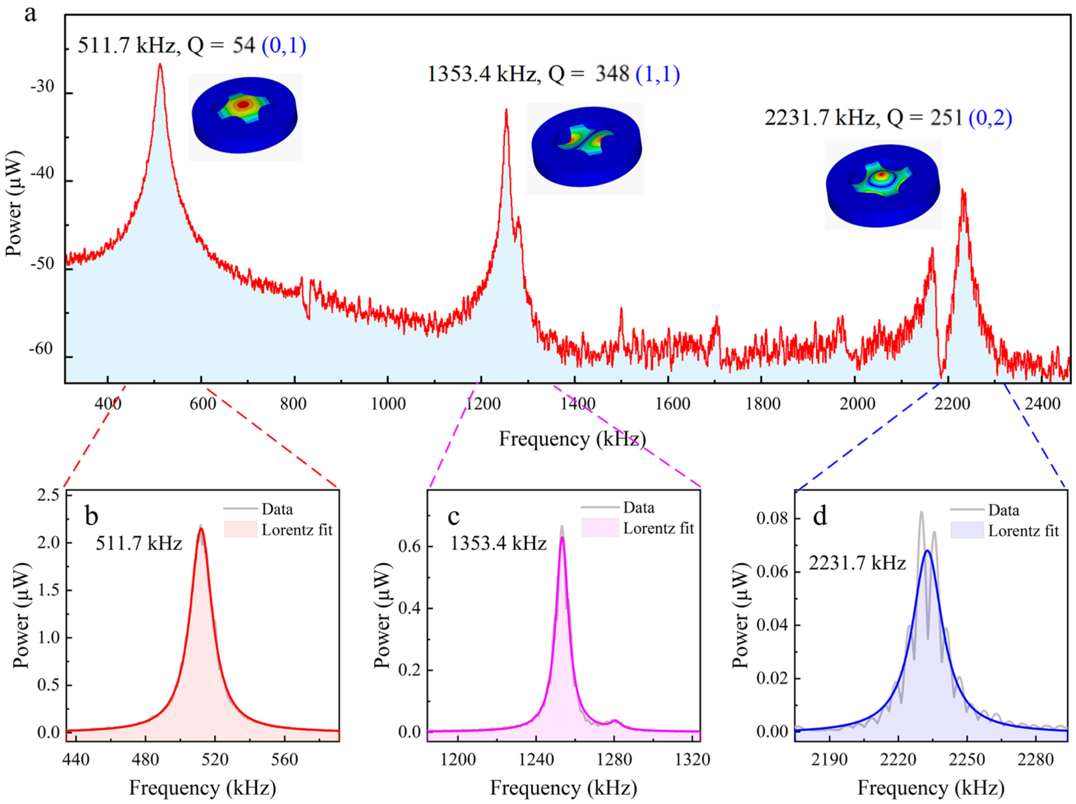

Figure 5. (a) Mechanical frequency characteristics and noise measurement of the sensors. Insets: the profiles of the (0,1) mode, (1,1) mode, and (0,2) mode (where the peaks occur) at 511.7, 1253.4, and 2231.7 kHz, respectively, obtained through finite element method simulation. (b)−(d) Lorentz fitting of the three resonance peaks in linear coordinates.

spring constant k_{eff}, results in a softening of the resonator.[32] The resonant frequency calculation formula is

$$f = \frac{1}{2\pi}\sqrt{k_{\mathrm{eff}}/m_{\mathrm{eff}}} \qquad (1)$$

where m_{eff} is the effective mass of the resonator. The negative detuning of the k_{eff} results in blue detuning of the resonant frequencies.

3.2. Hydrogen Gas Sensing Mechanism.

The sensing mechanism of the sensor for gas detection is as follows: In a hydrogen atmosphere, the Pd on the nanofilm from a metal to a metal hydride (PdH_x) induces material lattice expansion.[33,34] This hydrogenation processing is reversible, and at the equilibrium state, the chemical expression is as follows:

$$\mathrm{Pd} + \frac{x}{2}\mathrm{H}_2 \leftrightarrow \mathrm{PdH}_x \qquad (2)$$

where x is the number of hydrogen atoms. When the Pd film dissociated absorbed hydrogen, the fixed parts of the trampoline nanofilm were constricted, and the suspended part of the film was stressed under compression in the longitudinal direction, resulting in lowering of the resonance frequencies. Upon absorbing hydrogen at a constant temper-

https://doi.org/10.1021/acsami.2c04105
ACS Appl. Mater. Interfaces 2022, 14, 29357−29365

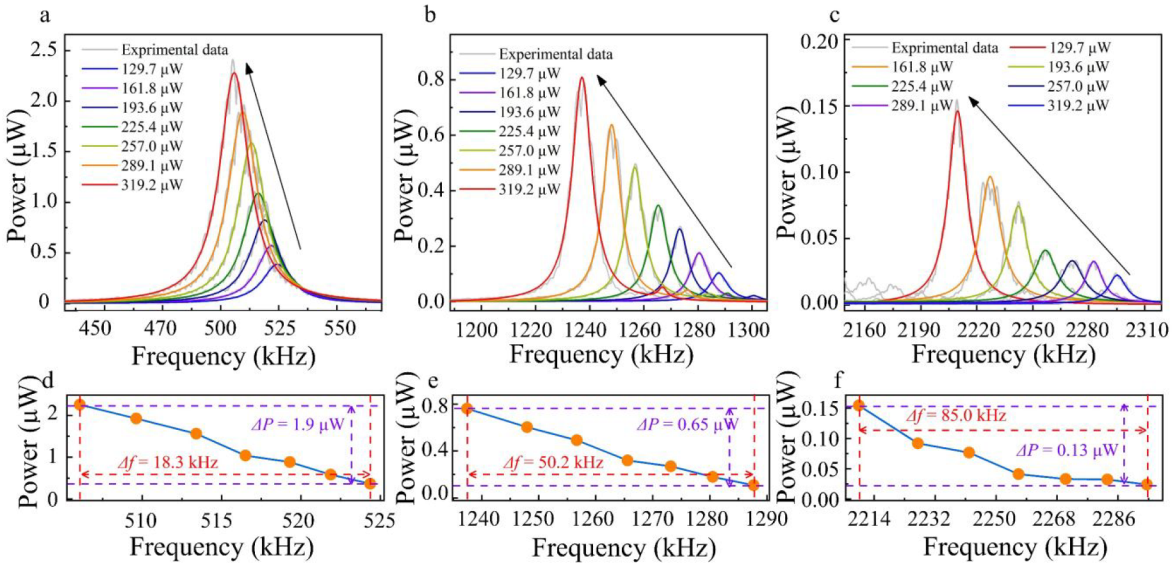

Figure 6. (a)−(c) Relationship between resonant frequencies and drive laser power of (0,1) mode, (1,1) mode, and (0,2) mode, respectively. (d)−(f) Plotted results of peak searching of Figure 6(a)−(c), respectively.

ature, the nanofilm's fundamental mechanical stress shifted the resonance frequency by the following:[10]

$$\Delta f_0 = \frac{Y f_0}{2\Delta\sigma(1 - \nu)} \tag{3}$$

where ν is the Poisson's ratio of the film, $\Delta\sigma$ is the hydrogen-related mechanical stress change, Y is the elastic modulus, and f_0 is the initial frequency. The hydrogen-related mechanical stress change can be given by the Stoneys equation:[35]

$$\Delta\sigma = \frac{E_{GA} t_{GA}^2}{6(1 - \nu_{GA}) t_{Pd}} \cdot \left(\frac{1}{R} - \frac{1}{R_0}\right) \tag{4}$$

where E_{GA}, ν_{GA}, and t_{GA} are the Young's modulus, Poisson's ratio and thickness of the graphene-Au composite film, respectively; t_{Pd} is the thickness of the Pd film; and R_0 and R are the radius of curvature of the graphene−Au-Pd composite film before and after hydrogen absorption, respectively.

3.3. Hydrogen Gas Sensing. The frequency response of the sensor (sample-1) was measured at different hydrogen concentrations at 22 °C. As shown in Figure 7a, the three mechanical resonant frequencies moved toward lower frequencies as the hydrogen gas concentration increased, and the degrees to which the three resonant frequencies shifted were different. When the hydrogen concentration was increased from 0 to 1000 ppm (v/v), the resonant frequencies at 511.7 kHz, 1253.4 kHz, and 2231.7 kHz blue-shifted 100.4 kHz, 257.5 kHz, and 400.6 kHz, respectively. Figure 7b−d shows the detailed evolution of the three resonant frequencies from the sensor as the hydrogen gas concentration increased. Each measurement was gathered over 10 min to ensure absorption equilibrium was reached. For clarity, the data of hydrogen adsorption equilibrium concentration vs frequency shift of three resonant frequencies are plotted in Figure 7e. Notably, the sensor has a higher sensitivity at higher resonant frequencies; thus, we used the most sensitive resonant frequency @2.23 MHz to test the 20 and 40 ppm concentrations, as shown by the green data in Figure 7e. The y-error bar in Figure 7e represents the standard deviation of six measurements at each concentration and the constraint on the spectrum resolution bandwidth (RBW), which was set to 3 kHz. The x-error represents the gas concentration control error. To evaluate the hydrogen-induced resonant frequency responses of the three modes, we defined the figure of merit (FOM) as $\Delta f_{res} Q / f_{res}$, the resonant frequency as f_{res}, the mechanical Q factor as Q, and the frequency shifted as the hydrogen concentration increased from 0 to 1000 ppm as $\Delta f_{res.}$

The LOD of the sensor can be evaluated by monitoring the frequency evolution over time. To record the frequency fluctuation of each mode at a hydrogen concentration of 100 ppm, we used a personal computer (PC) to control the FSA operation; the frequency of the drive laser was swept, and the spectrum was recorded every minute for half an hour. Restricted by the RBW of the FSA, the fluctuation of the three modes was not obvious; thus, the data in Figure 7f are the results of peak searching after Lorentz fitting of the experimental data. The frequency fluctuation could be attributed to the instability of drive laser, thermomechanical noise, temperature fluctuation, adsorption−desorption noise, and instrumentation noise. The standard deviations (σ) of the frequency fluctuations of the (0,1) mode, (1,1) mode, and (0,2) mode were 0.319 kHz, 0.662 kHz, and 1.382 kHz, respectively. The 1σ-LODs of the three modes were 896 ppb, 741 ppb, and 882 ppb.

The performance statistics of the sensor proposed in this article are summarized in Table 1. If measured via FSA with a resolution of a few tens of Hz, the fiber-optic compact all-optical hydrogen sensor based on optomechanical resonant nanofilm approaches can obtain a wide dynamic range of approximately 4 orders of magnitude for hydrogen gas, an important chemical compound in industrial and safety monitoring. To the best of the authors' knowledge, 741 ppb is the lowest LOD micro/nanoscale fiber-optic hydrogen sensor ever reported, which represents two order magnitude improvement over previously reported work.[23] The performances of several compact fiber-optic hydrogen sensors are summarized in SI Table S1.

To investigate the temporal response of the hydrogen sensor, we recorded the power at 411 kHz (the resonance frequency of the fundamental mode at a 1000 ppm

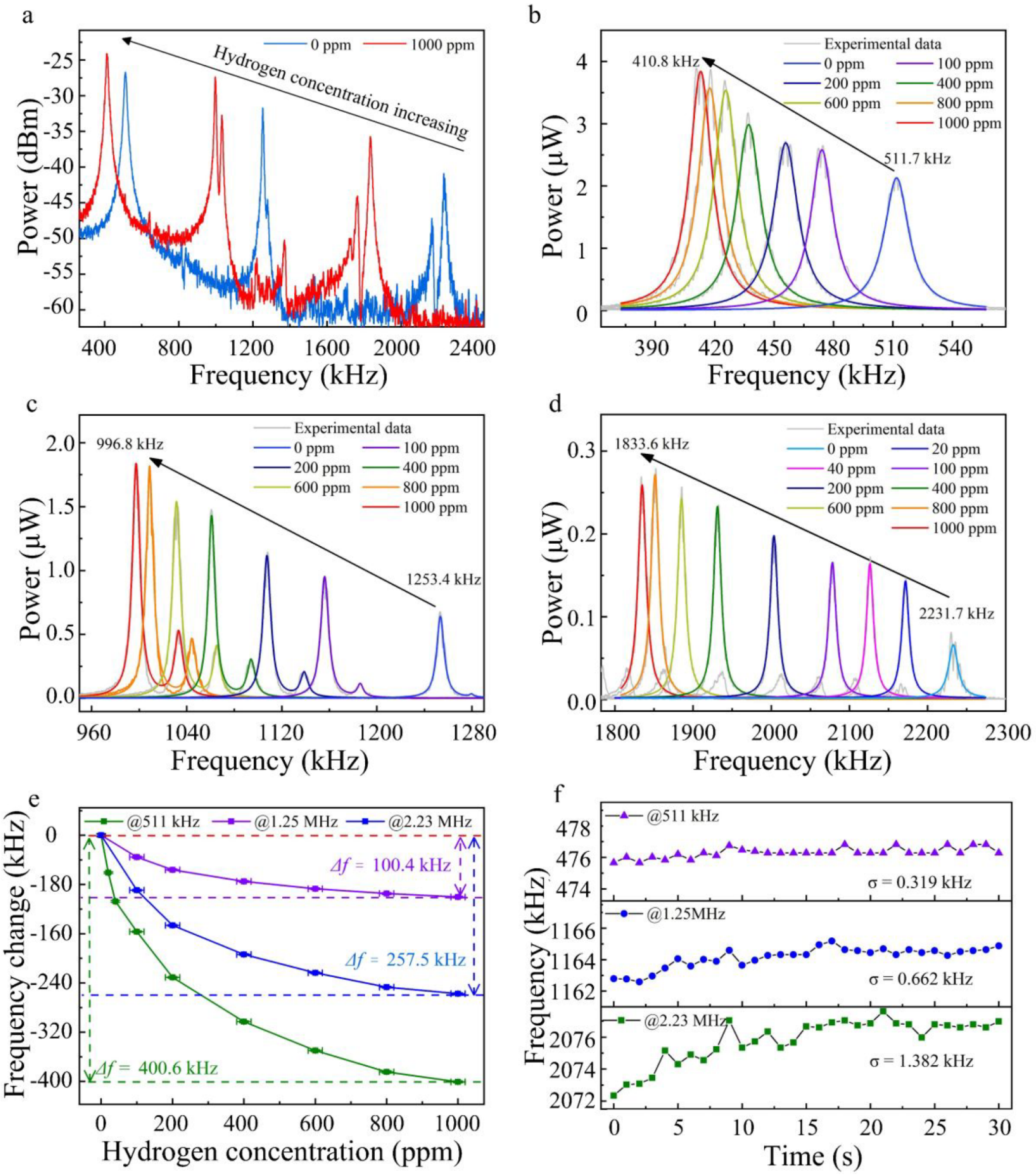

Figure 7. (a) Frequency characteristic of the sensor at hydrogen concentrations of 0 and 1000 ppm. (b)−(d) Evolution of the three resonant frequencies shifting in response to different hydrogen concentrations. (e) Plotted frequency shifts of the three modes vs hydrogen concentration. (f) Fluctuations in the resonant frequencies of the three modes at 100 ppm hydrogen concentration.

Table 1. Performance Statistics of the Sensor

resonant frequency (kHz)	mechanical Q factor	1000 ppm hydrogen-induced shift (kHz)	FOM ($\Delta f_{\text{res}}Q/f_{\text{res}}$)	LOD (ppb)
511.7	54	100.4	10.6	869
1253.4	348	257.4	66.2	741
2231.7	251	400.6	45.1	882

concentration) in the time domain at different hydrogen concentrations, as shown in Figure 8a. The green areas in the figure indicate that the sensor was exposed to a concentration of hydrogen, while the gray areas indicate that it was exposed to pure nitrogen. The response time at the 20 ppm concentration was also measured. Because the sensor has a longer response time at low concentrations, the frequency response of the sensor's response to hydrogen at concentrations of 20 and 40 ppm can be recorded by PC-controlled FSA with 30 s intervals. Time-dependent data of the spectrum of the sensor at different hydrogen concentrations were plotted into a color map, as shown in Figure 8b. For clarity, the red line in Figure 8b shows the results of peak searching the data. The temporal response of the sensor was measured by recording one frequency power. Figure 8c shows the power measured at 2172.37 kHz in the time domain in 20 ppm hydrogen concentrations. As the hydrogen concentration increased, the power at 2173.37 kHz changed with of the resonant frequency shifted to a lower frequency, then reach steady. Figure 8d shows the power measured at 411 kHz in the time domain in the test of 1000 ppm hydrogen concentrations. Here, the sensor response and recovery time are defined as the time required for the sensor to reach 90% of its steady power state response. The response and recovery time are 120.3 s and 91.3 s at a 1000 ppm hydrogen concentration. The response time vs hydrogen concentration in the sensor is plotted in Figure 8e. The response time is longest when the concentration of hydrogen is 20 ppm, which is ~1170 s. The

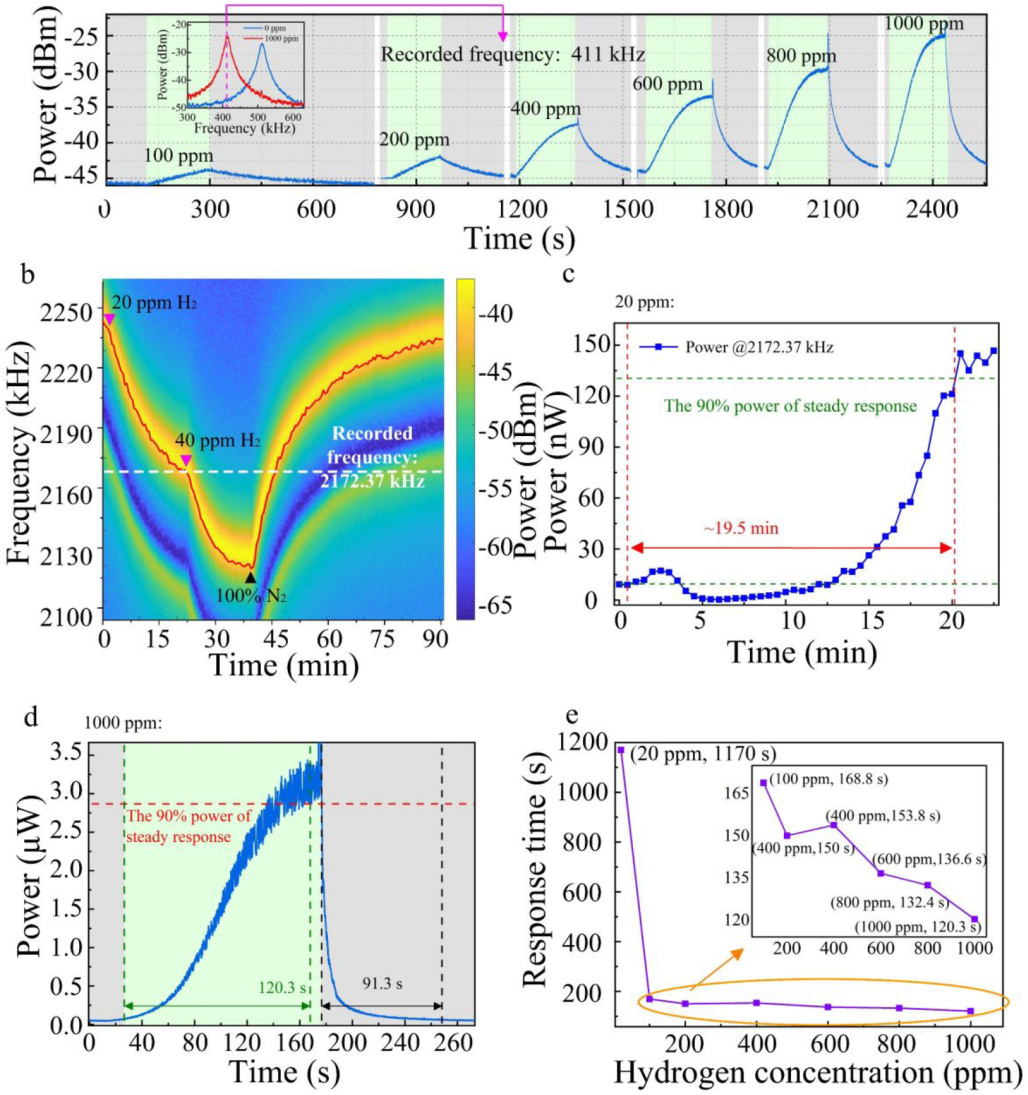

Figure 8. (a) Measured result of the power change in the time domain at different hydrogen concentrations. Here, 411 kHz is the resonant frequency of the fundamental mode at a 1000 ppm concentration. (b) Colored map of the mechanical frequency spectra varying in the range of 2093 kHz to 2265 kHz with the hydrogen concentration. (c) Temporal response at hydrogen concentrations of 20 ppm. (d) Response and recovery time at hydrogen concentrations of 1000 ppm. (e) Response time of the sensor for different hydrogen concentrations.

response time measured at the 1000 ppm hydrogen concentration is the shortest, which is ~120.3 s. Besides, the reproducibility of the hydrogen sensor was be investigated by recording the power change at 411 kHz for several cycles at different hydrogen concentrations, and the results are shown in Figure 9a−f. The measured results demonstrate that the sensor exhibits good recoverability and reproducibility.

4. CONCLUSION

In summary, we demonstrated an all-optical highly sensitive hydrogen sensor by actuating and measuring the resonant frequencies of an intricate Pd-decorated nanofilm resonator on a fiber end facet. While the hydrogen-induced Pd film expanded, the nanofilm was stressed under compression in the longitudinal direction, resulting in reduced resonance frequencies. Experimental results show that the fundamental, second and third resonant frequencies of the sensor exhibited nonlinear shifts of 100.4, 257.5, and 400.6 kHz, respectively, as the hydrogen concentration was varied from 0 to 1000 ppm (v/v) at room temperature. The sensor possesses high

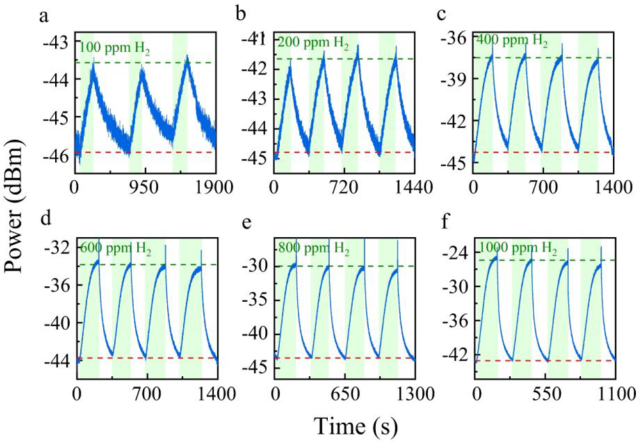

Figure 9. Sensor's repeatability is evaluated by recording the real-time power response of the sensor exposed to (a) 100 ppm, (b) 200 ppm, (c) 400 ppm, (d) 600 ppm, (e) 800 ppm, (f) 1000 ppm hydrogen concentrations for several cycles.

sensitivity, excellent repeatability and a low LOD of 741 ppb. In addition, the sensor fabrication is highly reproducible, paving the way for practical trace gas detection. From a wider perspective, this work builds the groundwork for integration of NOMS and fiber-optic devices to realize high-performance optical sensors. We anticipate this new technology can be applied in a wide range of disciplines, spanning from chemical sensing to cytomechanical sensing.

METHODS

Graphene Wet Transfer. The graphene was transferred to the end of the HCF with a wet transfer technique. The first step: detaching the graphene film from the Cu foil by placing the graphene/Cu sample onto a 0.075 g/mL $FeCl_3$ solution. The graphene/Cu sample floated on the surface of the $FeCl_3$ solution with Cu foil facing down. The second step: After the Cu foil was etched off, the $FeCl_3$ solution was carefully removed with an injection syringe and then injected with deionized water. The process was repeated 10 times to wash out the residual ions. The clean graphene film floated on the water. The third step: Moving the tip of the fiber toward the floating graphene film, dip it gently into the graphene film, and lift the fiber vertically from the water surface. The fourth step: As the residual water of the suspended graphene film on HCF evaporated, the graphene film remained firmly attached to the fiber tip end facet as a result of van der Waals force. The adhesion energies for multilayer graphene film with a SiO_2 substrate are large and comparable to solid liquid adhesion energies.[36] Therefore, the graphene film was strongly attached to the HCF end facet.

ASSOCIATED CONTENT

Supporting Information

The Supporting Information is available free of charge at https://pubs.acs.org/doi/10.1021/acsami.2c04105.

> Reproducibility of the proposed sensor, temperature sensitivity of the sensor, comparison with other hydrogen sensors (PDF)

AUTHOR INFORMATION

Corresponding Author

Shen Liu − *Key Laboratory of Optoelectronic Devices and Systems of Ministry of Education/Guangdong Province, College of Physics and Optoelectronic Engineering, Shenzhen University, Shenzhen 518060, China; Shenzhen Key Laboratory of Photonic Devices and Sensing Systems for Internet of Things, Guangdong and Hong Kong Joint Research Centre for Optical Fibre Sensors, Shenzhen University, Shenzhen 518060, China;* orcid.org/0000-0001-9266-2498; Email: shenliu@szu.edu.cn

Authors

Junxian Luo − *Key Laboratory of Optoelectronic Devices and Systems of Ministry of Education/Guangdong Province, College of Physics and Optoelectronic Engineering, Shenzhen University, Shenzhen 518060, China; Shenzhen Key Laboratory of Photonic Devices and Sensing Systems for Internet of Things, Guangdong and Hong Kong Joint Research Centre for Optical Fibre Sensors, Shenzhen University, Shenzhen 518060, China*

Peijing Chen − *Key Laboratory of Optoelectronic Devices and Systems of Ministry of Education/Guangdong Province, College of Physics and Optoelectronic Engineering, Shenzhen University, Shenzhen 518060, China; Shenzhen Key Laboratory of Photonic Devices and Sensing Systems for Internet of Things, Guangdong and Hong Kong Joint Research Centre for Optical Fibre Sensors, Shenzhen University, Shenzhen 518060, China*

Yanping Chen − *Key Laboratory of Optoelectronic Devices and Systems of Ministry of Education/Guangdong Province, College of Physics and Optoelectronic Engineering, Shenzhen University, Shenzhen 518060, China; Shenzhen Key Laboratory of Photonic Devices and Sensing Systems for Internet of Things, Guangdong and Hong Kong Joint Research Centre for Optical Fibre Sensors, Shenzhen University, Shenzhen 518060, China*

Junlan Zhong − *Key Laboratory of Optoelectronic Devices and Systems of Ministry of Education/Guangdong Province, College of Physics and Optoelectronic Engineering, Shenzhen University, Shenzhen 518060, China; Shenzhen Key Laboratory of Photonic Devices and Sensing Systems for Internet of Things, Guangdong and Hong Kong Joint Research Centre for Optical Fibre Sensors, Shenzhen University, Shenzhen 518060, China*

Yiping Wang − *Key Laboratory of Optoelectronic Devices and Systems of Ministry of Education/Guangdong Province, College of Physics and Optoelectronic Engineering, Shenzhen University, Shenzhen 518060, China; Shenzhen Key Laboratory of Photonic Devices and Sensing Systems for Internet of Things, Guangdong and Hong Kong Joint Research Centre for Optical Fibre Sensors, Shenzhen University, Shenzhen 518060, China*

Complete contact information is available at:
https://pubs.acs.org/10.1021/acsami.2c04105

Author Contributions

S.L. and J.L. jointly conceived the idea. S.L. and J.L. designed and fabricated the devices, built the experimental setup, and carried out the experiments. P.C. and Y.C. provided help for the experiment. J.L., S.L., and P.C. analyzed the data. J.L. wrote the manuscript with the help from S.L., J.Z. and Y.W. All authors have given approval to the final version of the manuscript.

Notes

The authors declare no competing financial interest.

ACKNOWLEDGMENTS

This study was supported by the National Natural Science Foundation of China (NSFC) (62175165); Guangdong Basic and Applied Basic Research Foundation (2021A1515011834); Shenzhen Science and Technology Program (Grant Nos. RCBS20200714114922296, JCYJ20210324120403009). We thank Xi Zhang from Electron Microscope Center of Shenzhen university for provide FIB processing services. We would furthermore thank Guoxuan Zhu and Bonan Liu for useful discussions.

REFERENCES

(1) Lassagne, B.; Garcia-Sanchez, D.; Aguasca, A.; Bachtold, A. Ultrasensitive Mass Sensing with a Nanotube Electromechanical Resonator. *Nano Lett.* **2008**, *8* (11), 3735−3738.

(2) Agache, V.; Blanco-Gomez, G.; Baleras, F.; Caillat, P. An Embedded Microchannel in a MEMS Plate Resonator for Ultrasensitive Mass Sensing in Liquid. *Lab Chip* **2011**, *11* (15), 2598−2603.

(3) Palyi, A.; Struck, P. R.; Rudner, M.; Flensberg, K.; Burkard, G. Spin-Orbit-Induced Strong Coupling of a Single Spin to a Nanomechanical Resonator. *Phys. Rev. Lett.* **2012**, *108* (20), 206811.

(4) Henriksson, J.; Villanueva, L. G.; Brugger, J. Ultra-low Power Hydrogen Sensing Based on a Palladium-coated Nanomechanical Beam Resonator. *Nanoscale* **2012**, *4* (16), 5059−5064.

(5) Dolleman, R. J.; Davidovikj, D.; Cartamil-Bueno, S. J.; van der Zant, H. S. J.; Steeneken, P. G. Graphene Squeeze-Film Pressure Sensors. *Nano Lett.* **2016**, *16* (1), 568−571.

(6) Miller, D.; Aleman, B. Spatially Resolved Optical Excitation of Mechanical Modes in Graphene NEMS. *Appl. Phys. Lett.* **2019**, *115* (19), 193102.

(7) Keskekler, A.; Shoshani, O.; Lee, M.; van der Zant, H. S. J.; Steeneken, P. G.; Alijani, F. Tuning Nonlinear Damping in Graphene Nanoresonators by Parametric-direct Internal Resonance. *Nat. Commun.* **2021**, *12* (1), 1−7.

(8) Lee, J.; Wang, Z.; He, K.; Yang, R.; Shan, J.; Feng, P. X. L. Electrically Tunable Single- and Few-layer MoS2 Nanoelectromechanical Systems with Broad Dynamic Range. *Sci. Adv.* **2018**, *4* (3), No. eaao6653.

(9) Chae, J.; An, S.; Ramer, G.; Stavila, V.; Holland, G.; Yoon, Y.; Talin, A. A.; Allendorf, M.; Aksyuk, V. A.; Centrone, A. Nanophotonic Atomic Force Microscope Transducers Enable Chemical Composition and Thermal Conductivity Measurements at the Nanoscale. *Nano Lett.* **2017**, *17* (9), 5587−5594.

(10) Blaikie, A.; Miller, D.; Aleman, B. J. A Fast and Sensitive Room-temperature Graphene Nanomechanical Bolometer. *Nat. Commun.* **2019**, *10* (1), 1−8.

(11) Liu, X.; Ma, T.; Pinna, N.; Zhang, J. Two-Dimensional Nanostructured Materials for Gas Sensing. *Adv. Funct. Mater.* **2017**, *27* (37), 1702168.

(12) Joshi, N. J.; Braunger, M. L.; Shimizu, F. M.; Riul Jr, A.; de Oliveira Jr, O. N. Insights into Nano-heterostructured Materials for Gas Sensing: A Review. *Multifunct. Mater.* **2021**, *4*, 032002.

(13) Schlicke, H.; Behrens, M.; Schroeter, C. J.; Dahl, G. T.; Hartmann, H.; Vossmeyer, T. Cross-Linked Gold-Nanoparticle Membrane Resonators as Microelectromechanical Vapor Sensors. *Acs Sens.* **2017**, *2* (4), 540−546.

(14) Steeneken, P. G.; Dolleman, R. J.; Davidovikj, D.; Alijani, F.; van der Zant, H. S. J. Dynamics of 2D Material Membranes. *2d Mater.* **2021**, *8* (4), 042001.

(15) Roslon, I. E.; Dolleman, R. J.; Licona, H.; Lee, M.; Siskins, M.; Lebius, H.; Madauss, L.; Schleberger, M.; Alijani, F.; van der Zant, H. S. J.; Steeneken, P. G., High-frequency Gas Effusion through Nanopores in Suspended Graphene. *Nat. Commun.* **2020**, *11* (1). DOI: 10.1038/s41467-020-19893-5

(16) Drmosh, Q. A.; Yamani, Z. H.; Hendi, A. H.; Gondal, M. A.; Moqbel, R. A.; Saleh, T. A.; Khan, M. Y. A Novel Approach to Fabricating a Ternary rGO/ZnO/Pt System for High Performance Hydrogen Sensor at Low Operating Temperatures. *Appl. Surf. Sci.* **2019**, *464*, 616−626.

(17) Mirzaei, A.; Sun, G.-J.; Lee, J. K.; Lee, C.; Choi, S.; Kim, H. W. Hydrogen Sensing Properties and Mechanism of NiO-Nb2O5 Composite Nanoparticle-based Electrical Gas Sensors. *Ceram. Int.* **2017**, *43* (6), 5247−5254.

(18) Motaung, D. E.; Mhlongo, G. H.; Makgwane, P. R.; Dhonge, B. P.; Cummings, F. R.; Swart, H. C.; Ray, S. S. Ultra-high Sensitive and Selective H-2 Gas Sensor Manifested by Interface of n-n Heterostructure of CeO2-SnO2 Nanoparticles. *Sens. Actuators, B* **2018**, *254*, 984−995.

(19) Lee, J. H.; Kim, J. Y.; Kim, J. H.; Mirzaei, A.; Kim, H. W.; Kim, S. S. Pd-decorated Si Nano-horns as Sensitive and Selective Hydrogen Gas Sensors. *Mater. Res. Bull.* **2020**, *132*, 110985.

(20) Xu, H.; Liu, Y.; Liu, H.; Dong, S.; Wu, Y.; Wang, Z.; Wang, Y.; Wu, M.; Han, Z.; Hao, L. Pd-decorated 2D SnSe Ultrathin Film on SiO2/Si for Room-temperature Hydrogen Detection with Ultrahigh Response. *J. Alloy. Compd.* **2021**, *851*, 156844.

(21) Liu, Q.; Yao, J.; Wu, Y.; Wang, Y.; Ding, G. Two Operating Modes of Palladium Film Hydrogen Sensor based on Suspended Micro Hotplate. *Int. J. Hydrogen Energy* **2019**, *44* (21), 11259−11265.

(22) Patton, J. F.; Hunter, S. R.; Sepaniak, M. J.; Daskos, P. G.; Smith, D. B. Rapid Response Microsensor for Hydrogen Detection using Nanostructured Palladium Films. *Sens. Actuator, A* **2010**, *163* (2), 464−470.

(23) Ma, J.; Zhou, Y.; Bai, X.; Chen, K.; Guan, B.-O. High-sensitivity and Fast-response Fiber-tip Fabry-Perot Hydrogen Sensor with Suspended Palladium-decorated Graphene. *Nanoscale* **2019**, *11* (34), 15821−15827.

(24) Luo, J.; Liu, S.; Chen, P.; Lu, S.; Zhang, Q.; Chen, Y.; Du, B.; Tang, J.; He, J.; Liao, C.; Wang, Y. Fiber Optic Hydrogen Sensor based on a Fabry-Perot Interferometer with a Fiber Bragg Grating and a Nanofilm. *Lab Chip* **2021**, *21* (9), 1752−1758.

(25) Tittl, A.; Mai, P.; Taubert, R.; Dregely, D.; Liu, N.; Giessen, H. Palladium-Based Plasmonic Perfect Absorber in the Visible Wavelength Range and Its Application to Hydrogen Sensing. *Nano Lett.* **2011**, *11* (10), 4366−4369.

(26) She, X.; Shen, Y.; Wang, J.; Jin, C. Pd Films on Soft Substrates: a Visual, High-contrast and Low-cost Optical Hydrogen Sensor. *Light Sci. Appl.* **2019**, *8*, 1−10.

(27) Castellanos-Gomez, A.; van Leeuwen, R.; Buscema, M.; van der Zant, H. S. J.; Steele, G. A.; Venstra, W. J. Single-Layer MoS2Mechanical Resonators. *Adv. Mater.* **2013**, *25* (46), 6719−6723.

(28) Barton, R. A.; Ilic, B.; van der Zande, A. M.; Whitney, W. S.; McEuen, P. L.; Parpia, J. M.; Craighead, H. G. High, Size-Dependent Quality Factor in an Array of Graphene Mechanical Resonators. *Nano Lett.* **2011**, *11* (3), 1232−1236.

(29) Miller, D.; Aleman, B. Shape Tailoring to Enhance and Tune the Properties of Graphene Nanomechanical Resonators. *2d Mater.* **2017**, *4* (2), 025101.

(30) Crowther, A. C.; Ghassaei, A.; Jung, N.; Brus, L. E. Strong Charge-Transfer Doping of 1 to 10 Layer Graphene by NO2. *ACS Nano* **2012**, *6* (2), 1865−1875.

(31) Davidovikj, D.; Slim, J. J.; Cartamil-Bueno, S. J.; van der Zant, H. S. J.; Steeneken, P. G.; Venstra, W. J. Visualizing the Motion of Graphene Nanodrums. *Nano Lett.* **2016**, *16* (4), 2768−2773.

(32) Arcizet, O.; Cohadon, P. F.; Briant, T.; Pinard, M.; Heidmann, A. Radiation-pressure Cooling and Optomechanical Instability of a Micromirror. *Nature* **2006**, *444* (7115), 71−74.

(33) Griessen, R.; Strohfeldt, N.; Giessen, H. Thermodynamics of the Hybrid Interaction of Hydrogen with Palladium Nanoparticles. *Nat. Mater.* **2016**, *15* (3), 311−317.

(34) Narayan, T. C.; Hayee, F.; Baldi, A.; Koh, A. L.; Sinclair, R.; Dionne, J. A. Direct Visualization of Hydrogen Absorption Dynamics in Individual Palladium Nanoparticles. *Nat. Commun.s* **2017**, *8*, 1−8.

(35) Wagner, S.; Kramer, T.; Uchida, H.; Dobron, P.; Cizek, J.; Pundt, A. Mechanical Stress and Stress Release Channels in 10−350 nm Palladium Hydrogen Thin Films with Different Micro-structures. *Acta Mater.* **2016**, *114*, 116−125.

(36) Koenig, S. P.; Boddeti, N. G.; Dunn, M. L.; Bunch, J. S. Ultrastrong Adhesion of Graphene Membranes. *Nat. Nanotechnol.* **2011**, *6* (9), 543−546.

■ NOTE ADDED AFTER ASAP PUBLICATION

This paper originally published ASAP on June 15, 2022. Minor corrections were made to Figures 3 and 5, and a new version was reposted on June 29, 2022.